Structural investigation of alkali aluminoborosilicate glass containing MoO_3 for vitrification of nuclear waste

Seon-Jin Kim[a], Tae-min Yeo[b], Sung-hee Hyun[c], Jisun Lee[b], Jung-Wook Cho[a, b, *]

[a]*Division of Advanced Nuclear Engineering, Department of Materials Science and Engineering, Pohang University of Science and Technology (POSTECH), Pohang, Gyeongbuk 37673, Republic of Korea*
[b]*Graduate Institute of Ferrous & Eco Materials Technology, Pohang University of Science and Technology (POSTECH), Pohang, 37673, Republic of Korea*
[c] *Steelmaking Research Group, POSCO, Pohang, 37859, Republic of Korea*
[*]*Corresponding author: jungwook@postech.ac.kr*

Keywords : nuclear waste glass, borosilicate glass, molybdenum, crystallization, glass structure

1. Introduction

Managing radioactive waste from nuclear power plants is crucial for environmental and human health safety. High-level radioactive waste (HLW), from reprocessed spent nuclear fuel, includes a complex mix of fission products, actinides, and other elements. Solidifying HLW into a stable form for secure storage is essential, with vitrification into chemically durable glass being an effective method. Aluminoborosilicate glass, used for HLW vitrification, offers high waste loading capacity and chemical durability. However, challenges arise due to the low solubility of certain ions (e.g., Mo^{6+}, $Tc^{4+/7+}$, SO_4^{2-}, U^{4+}), leading to potential crystallization and degradation. Molybdenum (Mo) often exists as Mo^{6+} in these glasses, forming isolated MoO_4^{2-} units that can induce micro-phase separation and nucleation of Mo-rich crystals, such as the soluble yellow phase (Na_2MoO_4). This study explores how different alkali cations affect Mo units in aluminoborosilicate glasses and their role in crystallization, using techniques like X-ray diffraction (XRD), field emission scanning electron microscopy (FE-SEM), X-ray absorption spectroscopy (XAS), X-ray photoelectron spectroscopy (XPS), Raman spectroscopy, differential scanning calorimetry (DSC), and solid-state MAS-NMR.

2. Methods and Results

2.1 Sample preparation

The SiO_2–B_2O_3–Al_2O_3–Na_2O–CaO system's nominal composition was based on SON68 glass, developed for high-level radioactive waste vitrification in France. Four samples were synthesized by adding Li_2O, Na_2O, K_2O, and Cs_2O, each with 2 mol% MoO_3.

Chemical mixtures of SiO_2, B_2O_3, Al_2O_3, Na_2CO_3, $CaCO_3$, Li_2CO_3, K_2CO_3, Cs_2CO_3, and MoO_3 (purity >99%) were pre-melted at 1200°C for 2 hours in a 95/5 Pt/Au crucible under atmospheric conditions. The resulting glass frits were ground and remelted at the same temperature for another 2 hours to ensure homogeneity. Samples were then cooled gradually at 1°C/min to room temperature to mimic natural cooling in industrial glass canisters, termed "slowly cooled" samples. Additionally, some samples were quenched on an oxygen-free copper plate for structural analysis.

Table I: Nominal composition of glasses (mol %).

	Li	Na	K	Cs
SiO_2	52.08	52.08	52.08	52.08
B_2O_3	14.88	14.88	14.88	14.88
Al_2O_3	3.72	3.72	3.72	3.72
CaO	5.58	5.58	5.58	5.58
Na_2O	16.74	21.74	16.74	16.74
Li_2O	5.00	0.00	0.00	0.00
K_2O	0.00	0.00	5.00	0.00
Cs_2O	0.00	0.00	0.00	5.00
MoO_3	2.00	2.00	2.00	2.00

2.2 X-ray Diffraction (XRD)

XRD analysis was conducted using a D8-Advance Davinci diffractometer (Bruker) with Cu–Kα radiation (λ = 0.15406 nm) at 40 kV and 40 mA. Pulverized samples were analyzed over a 2θ range of 5° to 55°, with a 0.020° step size and 96 s per step. The quenched glasses were confirmed to be amorphous, showing no crystalline peaks.

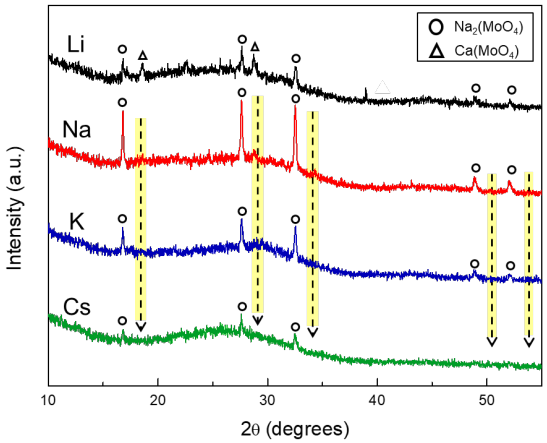

Fig. 1. XRD patterns of slowly cooled sample series.

XRD analyses of slowly cooled samples with Li, Na, K, and Cs are shown in **Fig. 1**. All samples, except for Li, exhibited the Na_2MoO_4 phase (JCPDS 01-073-7595). The Li sample also showed $CaMoO_4$ powellite phases (JCPDS 29-0351), though analyzing these peaks proved difficult. The intensity of Na_2MoO_4 diffraction peaks decreased as the alkali cation radius increased from Na to Cs. The Cs sample, in particular, showed very poor crystallization even with a slow cooling rate of 1 °C/min.

2.3 FE-SEM

Crystalline phase morphology was observed using FE-SEM (JSM-7100F, JEOL). Samples were cleaned ultrasonically, and surface chemical composition was analyzed with energy-dispersive X-ray spectroscopy (EDS, Aztec EDS, Oxford Instruments) attached to the SEM.

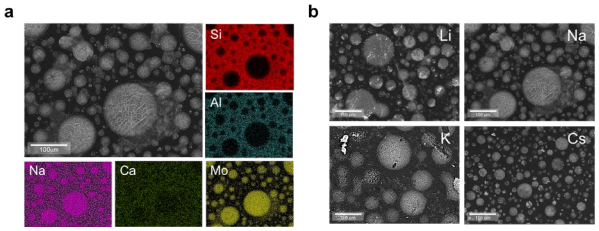

Fig. 2. SEM images of the surfaces of slowly cooled samples. (a) SEM images of the surface of the slowly cooled Na sample with EDS mapping for Si, Al, Mo, Na, and Ca. (b) SEM images of the surface of the slowly cooled sample series.

Fig. 2 shows the SEM image and EDS analysis of a slowly cooled sample. **Fig. 2a** highlights a phase rich in Na and Mo, indicating Na_2MoO_4 formation, consistent with XRD results. Although XRD detected $CaMoO_4$ in Li samples, EDS analysis found no Ca-containing crystals. The sample surface, shown in **Fig. 2b**, displays a uniform distribution of spherical Na_2MoO_4 crystals. SEM reveals sparse crystal distribution inside the sample, suggesting Na_2MoO_4 crystals underwent liquid-liquid phase separation during cooling. Despite identical thermal conditions, crystal sizes varied notably: Cs samples ranged from 20 to 50 μm, while other samples generally exceeded 100 μm.

2.4 XAS

XAS data at the Mo K-edge were collected at the Pohang Light Source, South Korea, using a Si (111) monochromator and a ring current of 250 mA at 2.5 GeV. Quenched glass samples and references were analyzed in fluorescence mode, with EXAFS spectra recorded from 19,900 to 20,800 eV in 1 eV steps. Data analysis with ATHENA and ARTEMIS included transforming spectra to k-space, applying k2-weighting, and fitting with $S_0^2 = 0.92$ and $E_0 = 1.3$ eV. Fourier transforms covered 3 $Å^{-1} \leq k \leq 10$ $Å^{-1}$ and 1.2 Å $\leq R \leq 3$ Å.

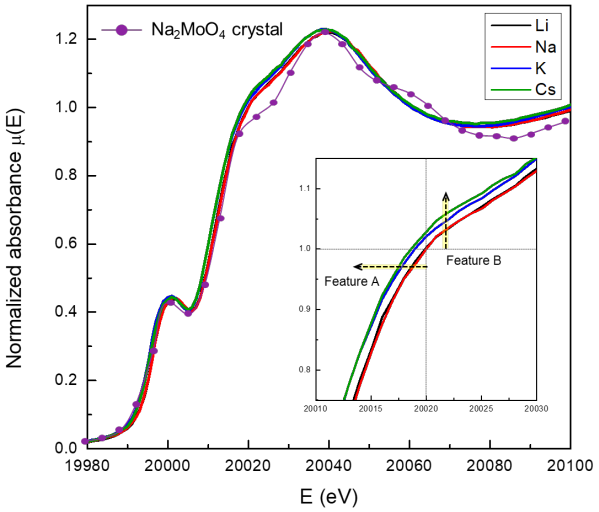

Fig. 3. Normalized Mo K-edge XANES spectra of the Na_2MoO_4 reference (purple dot) and quenched glasses containing MoO_3. The inset shows a magnified view of the XANES spectra on the region 20010 - 20030 eV.

Fig. 3 presents normalized Mo K-edge XANES spectra for the quenched glasses compared to Na_2MoO_4 crystals. The glasses' spectra, similar to Na_2MoO_4, exhibit slight broadening due to their amorphous nature, with a pre-edge peak around 20007 eV indicating tetrahedral MoO_4 geometry.

In the 20010 to 20030 eV range, Mo K-edge XANES spectra show an edge shift to lower energies (20020 to 20018.6 eV) in K and Cs glasses, suggesting partial Mo reduction. Feature B, associated with the 1s-5p transition, indicates Mo species with octahedral or distorted octahedral geometry. The edge shift and increased intensity in K and Cs glasses suggest Mo^{6+} may be partially reduced to Mo^{5+} or Mo^{4+}, or there is structural distortion due to increased coordination.

2.5 XPS

Mo 3d XPS analysis was conducted using a Nexsa-G2 (Thermo Fisher Scientific) with a monochromatic Al Kα source and 0.59 eV resolution. Spectra were collected with a pass energy of 50 eV and 0.1 eV step size, calibrated to the C 1s peak at 284.7 eV. Data were deconvoluted with OriginPro 8.1 using a Gaussian function to identify Mo oxidation states.

Mo oxidation states from +3 to +6 were analyzed using Mo 3d XPS (**Fig. 4**). The spectrum showed two main peaks: at 232.3 eV (Mo^{6+} $3d_{5/2}$) and 235.4 eV (Mo^{6+} $3d_{3/2}$), indicating Mo^{6+} as the dominant oxidation state in Li and Na glass samples. However, K and Cs glasses exhibited additional features not explainable by just these peaks. In K glass, an additional band for Mo^{5+} was observed ($3d_{3/2}$ at 234.3 eV, $3d_{5/2}$ at 231.2 eV), and

Cs glass showed a broad shoulder around 230 eV, suggesting Mo species in lower oxidation states (Mo^{5+} or Mo^{4+}). While Mo is typically found in the +6 state in borosilicate glasses, reduced Mo species have been reported in alkali borosilicate glasses. XPS confirmed Mo^{6+} in Li and Na samples, but additional bands in K and Cs glasses suggest the presence of reduced Mo species, consistent with XANES edge shifts (**Fig. 3**).

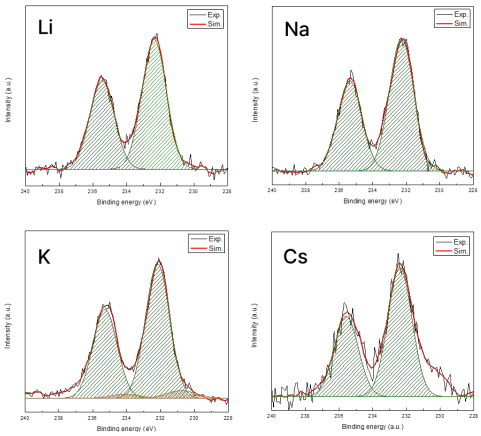

Fig. 4. Deconvoluted XPS spectra of Mo from quenched glasses.

2.6 Raman spectroscopy and glass transition temperature (T_g)

Raman spectroscopy was performed at room temperature using a LabRAM Aramis spectrometer (Horiba-Jobin-Yvonne) with a CCD detector. A 514 nm Ar-ion laser at 5 mW excitation power was used, with spectra collected for 300 s using a 50x objective on a 1 μm spot. The spectra ranged from 200 to 1600 cm^{-1} with a 1200 grooves/mm grating, achieving a resolution of about 1.5 cm^{-1}.

Glass transition temperatures (T_g) were measured using DSC (STA 1600, LABSYS evo). Approximately 60 mg of glass powder was heated at 10 K/min to 100 °C above its melting point, held isothermal for 5 minutes, then cooled and reheated at 10 K/min to determine T_g.

Fig. 5 shows Raman spectra normalized to the peak at 322 cm^{-1}, attributed to O–Mo–O bending vibrations in MoO_4^{2-} tetrahedra. Significant peaks at 855 and 900 cm^{-1} correspond to asymmetric and symmetric Mo–O stretching vibrations, indicating tetrahedral Mo coordination in aluminoborosilicate glass, consistent with EXAFS results. Despite low MoO_3 concentration, Mo's Raman sensitivity highlights a peak in the 800 to 1200 cm^{-1} range, obscuring silicate Q^n species vibrations. Shifts in Raman bands for silicate Q^3 species (1050 to 1100 cm^{-1}) with changing alkali cations suggest increased polymerization, as larger ions incorporate more bridging oxygens into SiO_4 units. This trend is supported by Neyret et al. and is reflected in the T_g, which rises from 501°C for Li to 544°C for Cs, indicating greater polymerization and structural rigidity.

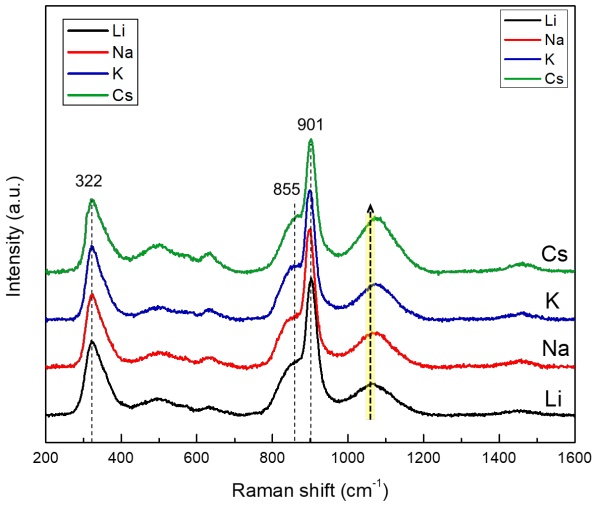

Fig. 5. Raman spectra obtained from quenched glass samples with various alkali cations.

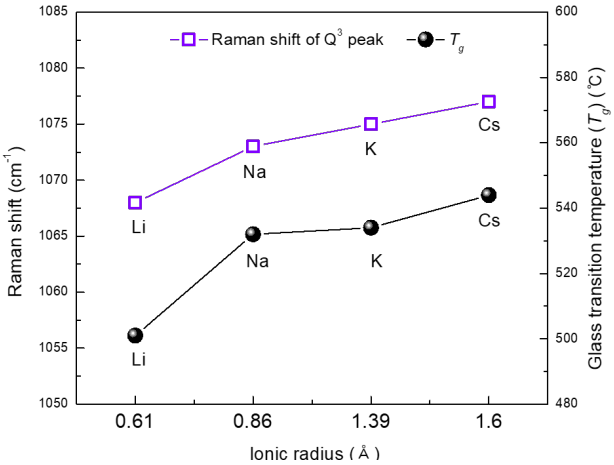

Fig. 6. Comparison of the Raman peak position around Q_3 region, and glass transition temperature (T_g) of each glass sample. Alkali ionic radii was calculated assuming that oxygen radius is 1.40 Å, from Shannon and Robert.

2.7 Solid-state MAS NMR

Solid-state MAS NMR was used to analyze the local structure around boron and aluminum with an Avance III HD NMR spectrometer. Samples were ground and analyzed at 10 kHz rotation speed in an 11.7 T magnetic field. For 11B MAS NMR, spectra were recorded at 160.45 MHz with 1024 scans, using a 2 mm rotor. 27Al MAS NMR was performed at 130.32 MHz with 2048 scans using a 4 mm rotor. Chemical shifts were calibrated against 1 M boric acid and AlCl3, respectively, and analyzed using DMFit software.

^{11}B and ^{27}Al MAS NMR spectra were analyzed to investigate the structural units in glass. **Fig. 7** shows that all glasses exhibit two main features in the ^{11}B spectra: a broad peak at ~15 ppm for BO_3 units and a peak at ~0 ppm for BO_4 units, indicating a predominance of BO_4. As the alkali cation radius increases from Li to Cs, there is a slight decrease in

BO_4 units, but the differentiation between borate units remains largely unaffected. **Fig. 8** reveals that the ^{27}Al NMR spectra have an asymmetric peak around 60 ppm, corresponding mainly to AlO_4 units, with minor AlO_5 and AlO_6. This consistent peak suggests that varying alkali cation sizes do not significantly alter aluminum's structural role in the glass.

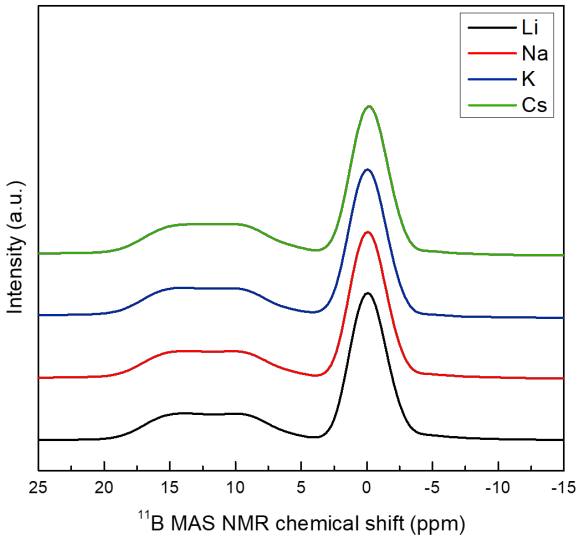

Fig. 7. Normalized ^{11}B MAS NMR spectra of the quenched glass samples. Inset shows magnified view of the spectra in 20–5 ppm range.

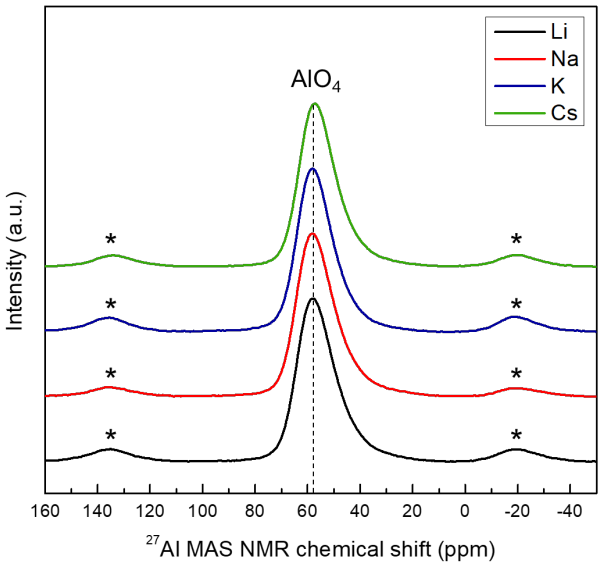

Fig. 8. ^{27}Al MAS NMR spectra of the quenched glass samples.

2.8 Discussion

Raman spectroscopy and T_g measurements reveal changes in glass polymerization across different alkali glasses, consistent with XRD and SEM results. The crystallization tendency of Na_2MoO_4 decreases with increasing alkali cation radius from Na to Cs, suggesting better MoO_3 solubility. Initial hypotheses considered changes in Al and B units as drivers for polymerization, but ^{11}B and ^{27}Al NMR spectra showed minimal impact of alkali cations on these structural units. Instead, increased BO_3 fractions with larger cations suggest that polymerization is influenced by Si rather than Al or B.

Larger alkali cations like K and Cs enhance network polymerization by modifying the glass structure. These cations act as network modifiers, reducing Mo diffusion and affecting the formation of MoO_4^{2-} units. This results in an environment where MoO_4^{2-} units are less likely to form due to decreased non-bridging oxygens (NBOs), which are essential for their formation.

Two hypotheses explain how Mo integrates into the silicate network. First, Mo cations may form octahedral MoO_6^{6-} units with weaker bonds, supported by increased XANES peak intensity for distorted octahedral sites. This integration is feasible due to reduced bond valence, enabling Mo to connect with the silicate network. Second, Mo may reduce to lower oxidation states (Mo^{5+} or Mo^{4+}) in response to NBO deficiencies, as suggested by XANES and XPS spectra showing broad features not attributable to Mo^{6+}.

The study concludes that the addition of large alkali cations creates an NBO-deficient environment, leading to the formation of Mo species that integrate into the silicate network, either as MoO_6^{6-} or reduced Mo species. This structural change helps delay MoO_3 crystallization and enhances the network's rigidity, as illustrated in proposed structural models.

3. Conclusions

This study analyzed aluminoborosilicate glasses with various alkali cations (Li, Na, K, Cs) to enhance MoO_3 solubility. Results show that larger alkali cations reduce Na_2MoO_4 crystallization. Raman spectra and T_g data indicate increased network polymerization with larger alkali ions. NMR results suggest that changes are related to the silicate network, not boron or aluminum. Large alkali cations create an NBO-deficient environment, leading to structural modifications in molybdenum, either transforming it to MoO_6^{6-} or forming reduced Mo species. These modifications inhibit MoO_4^{2-} crystallization, enhancing Mo solubility in the glass.

Acknowledgments

This paper is a result of The Human Resources Development Project for HLW Management hosted by KORAD and MOTIE.

REFERENCES

[1] Caurant, D.; Majérus, O. Glasses and Glass-Ceramics for Nuclear Waste Immobilization. In Encyclopedia of Materials: Technical Ceramics and Glasses; Elsevier, 2021; pp 762–789.
[2] Nicoleau, E.; Schuller, S.; Angeli, F.; Charpentier, T.; Jollivet, P.; Le Gac, A.; Fournier, M.; Mesbah, A.; Vasconcelos, F. Phase Separation and Crystallization Effects on the Structure and Durability of Molybdenum Borosilicate Glass. Journal of Non-Crystalline Solids 2015, 427, 120–133.
[3] Caurant, D.; Majérus, O.; Fadel, E.; Lenoir, M.; Gervais, C.; Pinet, O. Effect of Molybdenum on the Structure and on the Crystallization of SiO 2 ?Na 2 O?CaO?B 2 O 3 Glasses. J American Ceramic Society 2007, 90 (3), 774–783.
[4] Ollier, N.; Charpentier, T.; Boizot, B.; Wallez, G.; Ghaleb, D. A Raman and MAS NMR Study of Mixed Alkali Na–K and Na–Li Aluminoborosilicate Glasses. Journal of Non-Crystalline Solids 2004, 341 (1–3), 26–34.
[5] Mabrouk, A.; Vaills, Y.; Pellerin, N.; Bachar, A. Structural Study of Lanthanum Sodium Aluminoborosilicate Glasses by NMR Spectroscopy. Materials Chemistry and Physics 2020, 254, 123492.
[6] Calas, G.; Le Grand, M.; Galoisy, L.; Ghaleb, D. Structural Role of Molybdenum in Nuclear Glasses: An EXAFS Study. Journal of Nuclear Materials 2003, 322 (1), 15–20.
[7] Sukenaga, Sohei, et al. "Incorporation limit of MoO3 in sodium borosilicate glasses." Journal of the American Ceramic Society 106.1 (2023): 293-305.
[8] Neyret, Muriel, et al. "Ionic transport of alkali in borosilicate glass. Role of alkali nature on glass structure and on ionic conductivity at the glassy state." Journal of Non-Crystalline Solids 410 (2015): 74-81.
[9] Gagné, Olivier Charles, and Frank Christopher Hawthorne. "Comprehensive derivation of bond-valence parameters for ion pairs involving oxygen." Acta Crystallographica Section B: Structural Science, Crystal Engineering and Materials 71.5 (2015): 562-578.